University of Bath

Alternative formats

If you require this document in an alternative format, please contact:
openaccess@bath.ac.uk

COMMUNICATION

Rational Design of a Two-Photon Fluorescent Probe for Human Cytochrome P450 3A and the Visualization of Mechanism-Based Inactivation

Jing Ning,[a,b,†] Zhenhao Tian,[c,†] Jiayue Wang,[b,d,†] Bo Wang,[e] Xiangge Tian,[b] Zhenlong Yu,[b] Xiaokui Huo,[b] Lei Feng,[a,f,*] Jingnan Cui,[g] Tony D. James,[f,h] and Xiaochi Ma[a,b,*]

Abstract: Mechanism-based inactivation (MBI) can mediate adverse reactions and hepatotoxicity from drugs, which is a result of their conversion into highly reactive metabolites catalyzed by enzymes such as cytochrome P450 3A (CYP3A). In the present research, we optimized the key interaction domain of the fluorophore with the target protein to develop a two-photon fluorescent probe for CYP3A enzymes that are involved in the metabolism of more than half of all clinical drugs. The developed **BN-1** probe exhibited appropriate selectivity and sensitivity for the semi-quantitative detection and imaging of endogenous CYP3A activity in various living systems, thereby providing a high-throughput screening system enabling evaluation of MBI-associated hepatotoxicity by CYP3A. Using **BN-1** as a fluorescent molecular tool facilitates the efficient discovery and characterization of CYP3A-induced MBI in natural systems.

[a]   Dr. J. Ning,[†] Prof. L. Feng, X. C. Ma
        Second Affiliated Hospital of Dalian Medical University
        Dalian 116023, China
        E-mail: leifeng@dmu.edu.cn (L. Feng); maxc1978@163.com (X. C. Ma)
[b]   Dr. J. Ning,[†] J. Y. Wang,[†] X. G. Tian, Z. L. Yu, X. K. Huo, Prof. X. C. Ma
        College of Integrative Medicine, College of Pharmacy
        Dalian Medical University
        Dalian 116044, China
[c]   Dr. Z. H. Tian[†]
        School of Life Sciences
        Northwestern Polytechnical University
        Xi'an, 710072, China
[d]   Dr. J. Y. Wang[†]
        Department of Pharmacy
        Peking University Shenzhen Hospital
        Shenzhen 518036, China
[e]   Dr. B. Wang
        School of Medicine & Holistic Integrative Medicine
        Nanjing University of Chinese Medicine
        Nanjing, China
[f]   Prof. L. Feng, T. D. James
        School of Chemistry and Chemical Engineering,
        Henan Normal University
        Xinxiang 453007, China
[g]   Prof. J. N. Cui
        State Key Laboratory of Fine Chemicals
        Dalian University of Technology
        Dalian 116024, China
[h]   Prof. T. D. James
        Department of Chemistry
        University of Bath
        Bath BA2 7AY, United Kingdom.

[†]   These authors contributed equally.

        Supporting information for this article is given via a link at the end of the document.

Mechanism-based inactivation (MBI) of enzymes converts an unreactive substrate into an active and electrophilic metabolite that causes the irreversible inhibition of target enzymes through covalent modification of key amino acid groups within the enzymatic catalytic cavity.[1] Unfortunately, the 'irreversible' and 'suicide' inhibition of a metabolizing enzyme induced by MBI is often associated with serious adverse sometimes life threatening drug reactions.[2] Compared with reversible inhibition, the MBI of metabolizing enzymes frequently causes unfavorable drug-drug interactions. Additionally, the formed active metabolites can initiate adverse pathways of drugs, since they can trigger irreversible covalent modification of biological macromolecules which ultimately results in toxicity.[3] This indirect effect is often more difficult to predict while being closely related to toxic events. For instance, aflatoxins can contaminate food and have been classified as a Group I carcinogen by the World Health Organization.[4] Many studies have indicated that their toxicity is primarily dependent on the CYP3A catalysis of aflatoxins producing extremely toxic epoxide metabolites which covalently bind to some key proteins and DNA, resulting in hepatotoxicity and DNA mutations.[5] Therefore, the discovery and assessment of the MBI of key metabolizing enzymes are of considerable significance for the development and safe use of medicines and public health.

Cytochrome P450 (CYP), part of a large superfamily of HEME-containing proteins, is a key family of enzymes involved in the first-passage metabolism of many exogenous substances in the human body.[6] One of the most important drug metabolizing enzymes in humans, CYP isoenzymes including CYP1A2, 2B6, 2C8, 2C9, 2C19, 2D6, 3A4 and 3A5 mediate the biotransformation of around 80% of therapeutic drugs.[6] Amongst these, CYP3A4 and CYP3A5, which can collectively be called CYP3A, are significantly expressed and distributed in the adult human liver,[7] and are involved in the metabolic clearance of more than half of all therapeutic drugs. Numerous drugs including HMG-CoA reductase inhibitors (statins), tyrosine kinase inhibitors (tinibs), and calcium channel blockers (dipines) are substrates of CYP3A.[8] Additionally, CYP3A is compatible with structurally diverse substrates resulting in high susceptibility to inhibition by co-administered drugs. Thereby, as the 'leader' in the metabolic processing of multiple market drugs, CYP3A is also the main 'victim' of MBI,[9] and CYP3A mediated MBI is often a primary factor in the evaluation of potentially unfavorable drug-drug interactions and toxicity effects.

Currently, the most common method to investigate MBI of CYP3A is to use specific substrates such as midazolam, with the aid of high-performance liquid chromatography and mass spectrometry (HPLC-MS).[10] However, these traditional methods have some problems such as low sensitivity and efficiency, and

they are unable to realize the detection in complex biological systems. In contrast, fluorescent probes exhibit many outstanding advantages including being ultrasensitive, often produce visual outputs, and are compatible with high-throughput screening and real-time monitoring.[11] Fluorescent probes are often regarded as molecular tools since they are suitable for evaluating complex biological effects mediated by target proteins such as CYPs.[12]

Over the past few years, several fluorescent probes for CYP3A have been developed and widely investigated.[13,14,15,16] Unfortunately, these fluorescent probes could not effectively detect the MBI of CYP3A in living biospecimens. For example, **DFB**, a 3,4-difluorobenzyl derivative of 3-hydroxy-5,5-dimethyl-4-(4-methylsulfonylphenyl)-(5H)-furan-2-one, exhibited a relatively high specificity toward CYP3A.[13] However, this probe failed to monitor the fluctuation of CYP3A activity in living cells or tissue, due to interference from the biological matrix under the fluorescence excitation and emission conditions. Additionally, **NEN** and **Hcy-Br** have been recently reported as isoform-specific probes for the selective sensing of CYP3A4 (**NEN**) or CYP3A5 (**Hcy-Br**) activity.[15] However, their applications towards the evaluation of mechanism-based CYP3A inhibition, however, has been limited by: 1) The substrate spectra of CYP3A4 and CYP3A5, although very similar, are not completely overlapping;[8] 2) The expression level of CYP3A4 and CYP3A5 and their proportions with respect to total CYP3A fluctuate significantly in individuals and within different biospecimens.[17] Therefore, fluorescent probes that separately detect CYP3A4 or CYP3A5, but not CYP3A4 and CYP3A5 together, cannot effectively evaluate the MBI of CYP3A. In other words, a single measurement of CYP3A4 or CYP3A5 activity may be inaccurate when uncovering the real MBI effect in a physiological environment. Therefore, it is important to develop fluorescent probes for sensitively monitoring CYP3A activity to discover and assess MBI-related biological effects.

The catalytic process between small molecular substrates and metabolic enzymes is complicated, which is embodied by the dynamic interaction during recognition, binding, and catalysis.[18] During the dynamic process, stable binding of the substrate in the enzymatic cavity is one of the key factors affecting the catalytic process. Therefore, in the present study, a strategy for optimization of fluorophore structure based on a modification of the key interaction domain of the fluorophore that affects stability of ligand binding was proposed.

7H-benzo[de]benzo[4,5]imidazo[2,1-a]isoquinolin-7-one (**BN**) was selected as a suitable fluorophore due to its known CYP binding ability[19] and prominent photo-physicochemical properties such as two-photon absorption and high fluorescence quantum yield.[20] On dissection of the key binding domain of the **BN** with CYP3A, it was found that the benzene ring of the benzimidazole (Head group, marked as b in light-green in Scheme 1A) plays an important role. This group of **BN** could significantly stabilize the fluorophore in the CYP3A active cavity facilitating the oxidative reaction (Scheme 1B). Therefore, the head group of **BN** was used as a crucial factor for rational optimization.

Subsequently, a series of derivatives were prepared by introducing alkyl or halogens to the head group of **BN** were designed and synthesized (Scheme 1C). 4-hydroxylation of **BN** and its derivatives introduces a hydroxyl group which is a strong electron donor in the D-π-A structure, resulting in CYP3A mediated fluorescence 'Switch-ON' of the substrates. Firstly, the catalytic activities of CYP3A toward the **BN** derivatives were
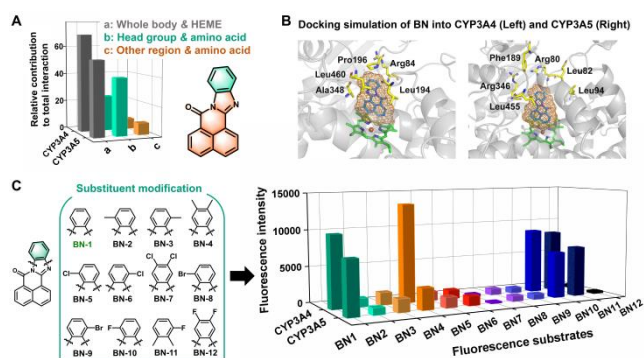
Scheme 1. Structure optimization of fluorophore (**BN**) according to its key interactions with CYP3A. (A) Relative contribution of the different regions of **BN** to stabilize **BN** in the catalytic cavity of CYP3A4 and CYP3A5. (B) Docking simulation of **BN** into CYP3A4 and CYP3A5, respectively. The amino acid residues that interacted with the 'Head' group of **BN** are shown. (C) The structures of **BN** derivatives and fluorescence response of **BN** derivatives at 526 nm (λ_{ex} = 470 nm) upon incubation with CYP3A4 and CYP3A5.

evaluated using the change in fluorescence intensity (Scheme 1C). The introduction of a halogen substituent including Cl and Br significantly influenced the hydroxylation of the fluorophore, confirming the impact of structural modifications of the 'head' group of **BN**. It was found that **BN-1**, **-10** and **-11** exhibited good reactivity toward both CYP3A4 and CYP3A5, and CYP3A4 exhibited a preference for **BN-4**. The varied catalytic activities of these **BN** derivatives could be explained by the calculated catalytic distances (Table S1) from the molecular simulations. A comprehensive evaluation of the fluorescence intensity and selectivity of the **BN** derivatives revealed that **BN-1** was a suitable molecular tool for the detection of CYP3A activity and MBI effects in various biological samples.

The specificity of **BN-1** for various CYP isoenzymes was then confirmed via in vitro assays. As shown in Figure 1B, CYP3A4/3A5 produced a remarkable fluorescence enhancement at 526 nm, over other CYP isoenzymes, after incubation with **BN-1**. Furthermore, the selectivity of **BN-1** in complex biological samples, such as human liver microsomes, was evaluated using a series of selective inhibitors of various CYP isoenzymes. The 'Switch-ON' of **BN-1** can be significantly inhibited by ketoconazole
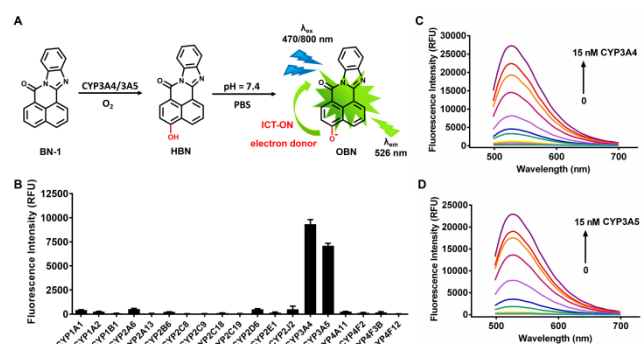

Figure 1. Fluorescence response of **BN-1** toward CYP3A. A) Proposed mechanism of CYP3A triggering the fluorescence response of **BN-1**. B) Fluorescence response of **BN-1** following incubation with various human CYPs. Data are shown as the mean ± S.D. (n = 3). Fluorescence spectra of **BN-1** following incubation with increasing concentrations of CYP3A4 (C) and CYP3A5 (D).

(KTZ, CYP3A selective inhibitor) (Figure S2). Additionally, various potential interfering species hardly effected the fluorescence response of **BN-1** (Figure S3). These results indicated that **BN-1** was highly selective for CYP3A even in complex systems.

Subsequently, the spectral properties of **BN-1** were evaluated. Above all, the metabolite of **BN-1** formed by CYP3A was identified as 4-hydroxy-7H-benzo[de]benzo[4,5]imidazo[2,1-a]isoquinolin-7-one (**HBN**), through comparison of the LC retention times, UV and MS spectra with those of a standard compound (Figure S4). The proposed mechanism of CYP3A triggering of the fluorescence response of **BN-1** is given in Figure 1A. **BN-1** exhibited extremely weak fluorescence over a wide pH range, while a high fluorescence output signal was produced by the hydroxyl product of **BN-1** (**HBN**) with a maximum intensity at 526 nm over pH range of 7-10 (λ_{ex} = 470 nm, Figure S5). Clearly, the distinct fluorescence response confirmed that CYP3A4/3A5-mediated the hydroxylation of **BN-1** introducing the hydroxyl group as a strong electron donor in the D–π–A structure, thereby increasing the intra-molecular charge transfer (Figure 1A). Upon the addition of CYP3A4 or CYP3A5, the fluorescence intensity increased at 526 nm (Figure 1C and 1D) and increased linearly when CYP3A4/3A5 were progressively added from 0 to 15 nM (Figure S6). Consequently, **BN-1** could be used to detect the CYP3A activity under physiological conditions.

The oxidation kinetic behavior of **BN-1** catalyzed by CYP3A4 and CYP3A5 was then characterized to reveal the interaction mode. The 4-hydroxylation of **BN-1** by CYP3A4, CYP3A5 and HLM obeyed the Michaeli-Menten equation (Figure S7). The K_m values for CYP3A4 and CYP3A5 mediated 4-hydroxylation were determined as 3.5 ± 0.5 and 10.1 ± 0.9 μM (Table S2).

The underlying mechanism for the interaction of **BN-1** with CYP3A4/3A5 was further elucidated using molecular dynamic simulations. The catalytic distance of **BN-1** and the catalytic center of HEME in CYP3A4/3A5 was calculated to be 3.1 and 3.5 Å, respectively (Table S1), which implied that there was a satisfactory interaction between CYP3A4/3A5 and **BN-1**, facilitating the hydroxylation reaction. The non-polar interaction between the 'head' group of **BN-1** and the HEME ring of CYP3A isoforms, probably the result of π-π stacking, stabilizes the binding of **BN-1** in the active cavity of CYP3A (Figure S1 and S8). Additionally, the predicted coordinate root-mean-square deviation (RMSD) value indicated the stability of **BN-1** bound with CYP3A4/3A5 (Figure S9). The polar interaction of the benzene head group of **BN-1** with Arg84 in CYP3A4, Arg80 and Arg346 in CYP3A5, respectively, can significantly contribute to molecular
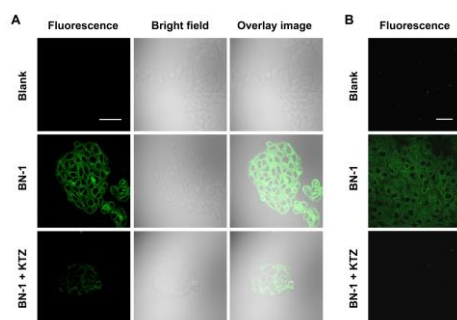
recognition and electrostatic interaction with CYP3A4/3A5.

The potential applicability of **BN-1** for the characterization of MBI was evaluated by exploring the response of **BN-1** for the selective CYP3A mechanism-based inactivator troleandomycin (TRO), using some non-fluorescent substrates of CYP3A including midazolam (MDZ) and testosterone (TST). As shown in Figure S10, the inactivation kinetic profile of TRO could be characterized using **BN-1**, and the inactivation constant K_i was determined to be 1.02 ± 0.23 μM. Furthermore, the inactivation kinetic profile and inactivation constant of TRO using **BN-1** was similar to that obtained using the two non-fluorescent substrates.

In order to demonstrate the potential of **BN-1** for the detection of CYP3A activity in living cells, differentiated HepaRG cells and rat primary hepatocytes were used in a fluorescence imaging assay. Prior to biological imaging using living cells, the cell viability of HepaRG in the presence of **BN-1** and **HBN** was evaluated using a CCK-8 assay. As shown in Figure S11, both **BN-1** and **HBN** exhibited low toxicity toward the living cells. Following incubation with **BN-1**, a strong fluorescence enhancement in differentiated HepaRG cells was observed (Figure 2A). Meanwhile, treatment with CYP3A selective inhibitor KTZ resulted in a significantly reduced fluorescence signal, implying that the turn-on fluorescence signal was triggered by endogenous CYP3A (Figure S12a). The bioimaging result of CYP3A in rat primary hepatocytes was similar to that observed in HepaRG cells (Figure S13). Furthermore, the two-photon fluorescence imaging of liver slice suggested the practicability of **BN-1** for tissue imaging of CYP3A (Figure 2B and S12b). The above-mentioned results confirmed that **BN-1** could be used to selectively measure endogenous CYP3A activity in biospecimens.
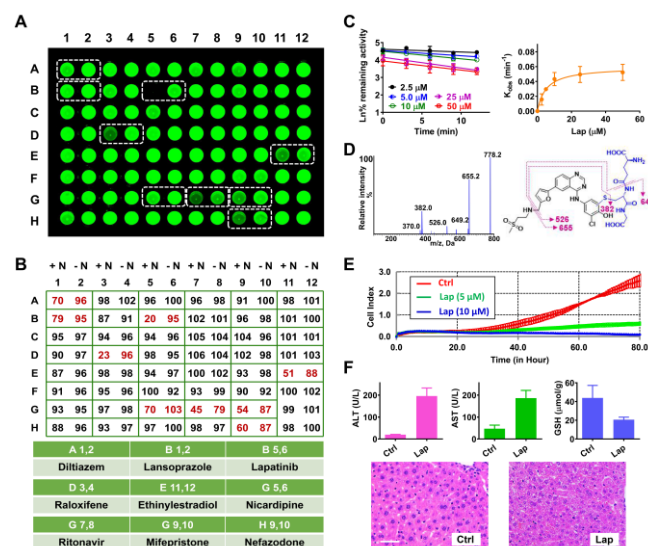
Figure 3. System for visual and high-throughput screening of mechanism-based CYP3A inactivation and MBI-induced hepatotoxicity evaluation of representative clinical drugs. Visual (A) and semi-quantitative (B) fluorescence response of **BN-1** towards the MBI by clinical drugs as assayed in 96-well microplates measured using a fluorescent image analyzer (λ_{ex}: 488 nm, λ_{em}: 570 ± 15 nm). The former of every two columns refers to the sample preincubated with NADPH (+N), and the latter refers to the corresponding sample preincubated with buffer (-N). The three independent results are shown in the supplementary data. (C) MBI kinetic of lapatinib (Lap, B5,6) against CYP3A. (D) MS/MS spectra and proposed structure of the GSH-adduct derived from Lap. (E) Label-free monitoring of the growth and viability of primary rat hepatocytes treated with Lap. (F) Liver damage is indicated by elevated ALT, AST serum levels and histological liver lesions in response to Lap in mice. Scale bar is 50 μm. Data are shown as the mean or mean ± S.D. (n = 3).

Figure 2. Two-photon fluorescence images of CYP3A activity in living specimen using **BN-1**. A) Differentiated HepaRG cells and B) rat liver tissue imaging when treated with **BN-1** in the present/absence of CYP3A inhibitor ketoconazole (KTZ). Excitation: 800 nm, emission window: 520 - 560 nm. Scale bar is 50 μm.

COMMUNICATION

The excellent selectivity and sensitivity of **BN-1** toward CYP3A indicated that **BN-1** facilitated the rapid, precise, and visual detection of CYP3A activity in complex biological samples, and thus ensured the systematic characterization of mechanism-based CYP3A inactivation. Initially, the *in vitro* incubation processes were optimized and confirmed using chemical drugs whose mechanism-based inhibitory effects had been previously reported (Scheme S1). Then, a high-throughput and visual assay for screening MBI of CYP3A was performed for 45 commonly used clinical drugs using a 96-well-microplate, and each drug was further divided into a NADPH-addition group (allowing the formation of potential active metabolites) or non-NADPH-addition group (non-metabolized) (Figure 3A, S14, Table S3). Subsequently, the percentage of residual activity for samples undergoing NADPH preincubation or not was calculated through quantitative analysis of the fluorescence signal, MBI is considered to exist in drugs that exhibits an activity loss of equal or greater than 15% after preincubation with NADPH (Figure 3B). Based on the fluorescence assay, the interaction between mechanism-based inactivator and CYP3A could be rapidly and visually characterized. Using lapatinib (Lap) as a positive example (B5,6 in Figure 3A), its inactivation constant K_i was determined to be 5.2 ± 1.5 µM (Figure 3C, Table S4). The reactive intermediate metabolite of CYP3A inactivator, a key factor in MBI of metabolizing enzymes and drug-induced liver injury, was further identified using a GSH trapping assay (Figure 3D). On the basis of this data, the MBI pathway of Lap toward CYP3A was proposed, and the formation of a quinone imine reactive intermediate was identified as the key aspect of this MBI process (Figure S15). Additionally, the hepatotoxicity of Lap was comprehensively evaluated using an *in vitro* toxicity and *in vivo* liver injury assay. As shown in Figure 3E, Lap could significantly inhibit the growth and viability of primary rat hepatocytes after 40 hours of treatment with 5 µM of Lap in comparison with the control group. Furthermore, Lap-induced liver injury was observed by elevated

ALT (alanine aminotransaminase), AST (aspartate aminotransferase) and histological liver lesions when compared with the control group (Figure 3F). All the above results demonstrated the reliability of the visual high-throughput screening system for mechanism-based CYP3A inactivation.

Our visual screening system exhibited many advantages such as high-efficiency and ultra-sensitivity for uncovering MBI of CYP3A within complex systems. Subsequently, as an example of a practical application, the screening system was used to track the MBI components of herbal medicines, and the screening strategy and flowchart are given in Figure 4A. It was found that *Euodia rutaecarpa* (Juss.) Benth. (E3,4), *Stephania tetrandra* S. Moore (B7,8), *Inula japonica* Thunb. (E7,8), *Ephedra sinica Stapf* (G7,8), *Xanthium sibiricum* Patr. (D9,10) and *Dioscorea bulbifera* L. (D11,12) exhibited MBI towards CYP3A (Figure 4B and S16, Table S5). Furthermore, the MBI components of *Euodia rutaecarpa* (Juss.) Benth. (ER) were successfully tracked and identified as limonin (Lim), evodiamine (Evo) and rutaecarpine (Rut) (Figure 4C). Benefiting from an accurate identification and high efficiency enrichment of the MBI components of ER, the interaction between Lim, Evo, Rut and CYP3A were characterized (Figure 4D and S17). The inactivation pathway for the three components was proposed (Figure 4E, and S18-20). As such, our high-throughput screening system for MBI could help to guide the discovery of toxic substances from food and drugs.

Subsequently, the MBI and liver injury effects of Lim, Evo and Rut were evaluated, in cellular, tissue and animal experiments (Figure S21). From which, it was found that **BN-1** could sensitively
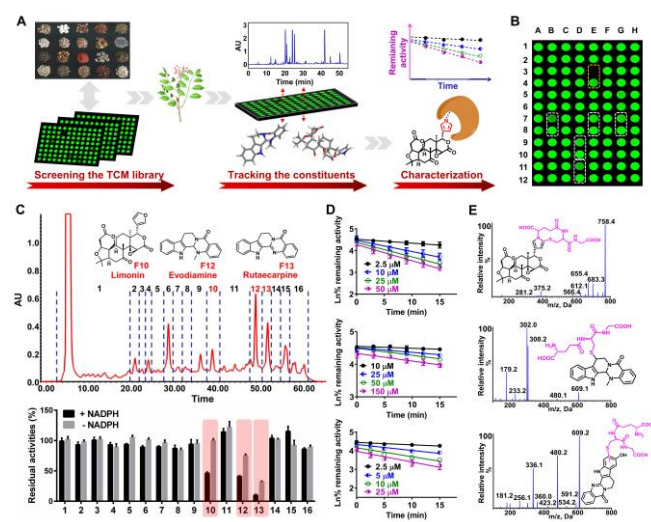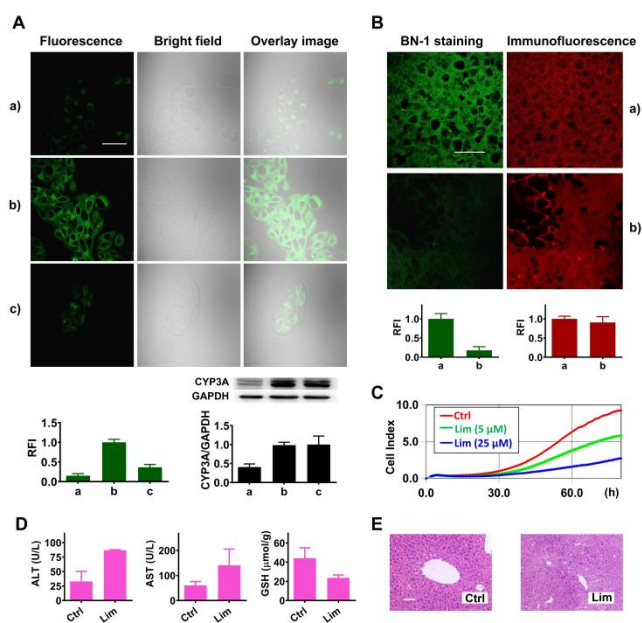

Figure 4. High-throughput and visual characterization of mechanism-based CYP3A inactivation of herbal medicines. (A) Flowchart of MBI molecular event characterization. (B) Visual fluorescence response to MBI components from herbal medicines in 96-well microplates using fluorescence image analyzer (λ_{ex}: 488 nm, λ_{em}: 570 ± 15 nm). Three independent results are shown in the supplementary data. (C) MBI tracking of *Evodia rutaecarpa* (Juss.) Benth. (D) MBI kinetics of Lim, Evo and Rut against CYP3A. (E) MS/MS spectra and proposed structure of the GSH-adduct derived from the three MBI components. Data are shown as the mean ± S.D. (n = 3).

Figure 5. MBI evaluation of Lim. (A) Two-photon fluorescence images of CYP3A activity in HepaRG (a), differentiated HepaRG (b), and Lim treated differentiated HepaRG (c) using **BN-1**. The average fluorescence intensity of images of CYP3A and the protein level of CYP3A in cells were analyzed. (B) Two-photon fluorescence images of CYP3A activity in rat liver slices using **BN-1** and CYP3A immunofluorescence of untreated (a) and treated (b) with Lim. RFI, relative fluorescence intensity. (C) Label-free monitoring of the growth and viability of primary rat hepatocytes treated with Lim. Liver damage in mice is indicated by elevated ALT, AST serum levels (D) and histological liver lesions (E) in response to Lim. Two-photon excitation: 800 nm, emission window: 520 - 560 nm. Immunofluorescence excitation: 559 nm, emission window: 610 - 650 nm. Scale bar is 50 µm. Data are shown as the mean ± S.D. (n = 3).

respond to variations of CYP3A expression and activity in HepaRG cells (Figure 5A). Then, to confirm the superior sensitivity of **BN-1** toward CYP3A-induced MBI, the fluorescence signal triggered by CYP3A activity in Lim-treated HepaRG cells and liver slices were analysed and compared with the semi-quantitative assay for CYP3A protein content including western blotting and immunofluorescence. It was found that **BN-1** could detect a significant decrease in CYP3A activity for differentiated HepaRG cells which were pretreated with Lim, while crucially, Lim did not affect the CYP3A protein levels (Figure 5A). Similar results were observed in the liver slice assay (Figure 5B). Overall, using **BN-1**, the MBI of CYP3A could be effectively evaluated using the detection of CYP3A activity. As expected, significant hepatotoxicity was observed when primary rat hepatocytes and experimental animals were treated with Lim, Evo and Rut, respectively (Figure 5C, 5D, 5E and S22-23). The above results confirmed that **BN-1** could be used for tracking of mechanism-based CYP3A inactivation in complex systems, facilitating an assessment of the toxicity risk of exogenous chemicals.

In summary, using a rational molecular design strategy, we have developed and synthesized a two-photon fluorescent probe **BN-1** for CYP3A. **BN-1** exhibits excellent CYP3A specificity and imaging capability, making it suitable for the semi-quantitative detection and imaging of CYP3A4 in various living systems. As such **BN-1** provides a solid foundation for constructing systems suitable for use in high-throughput screening and evaluation MBI-associated hepatotoxicity. In summary, we anticipate that **BN-1** could be used as a molecular tool to discover and characterize the MBI of CYP3A in biological systems.

[1] a) R. B. Silverman, *Methods Enzymol.* **1995**, *249*, 240-283; b) R. B. Silverman, *Chem. Rev.* **2018**, 118, 4037-4070.

[2] Z. W. Zhou, S. F. Zhou, *Expert Opin. Drug Metab. Toxicol.* **2009**, 5, 579-605.

[3] S. Feng, X. He, *Curr. Drug Metab.* **2013**, 14, 921-945.

[4] a) World Health Organization International Agency for Research on Cancer: IARC Monographs on the Evaluation of Carcinogenic Risks to Humans, **2002**, 82, 171; b) J. W. Bennett, M. Klich, *Clin. Microbiol. Rev.* **2003**, 16, 497-516.

[5] V. Dohnal, Q. H. Wu, K. Kuča, *Arch. Toxicol.* **2014**, 88, 1635-1644.

[6] a) W. E. Evans, M. V. Relling, *Science* **1999**, 286, 487-491; b) P. Wei, J. Zhang, M. Egan-Hafley, S. Liang, D. D. Moore, *Nature* **2000**, 407, 920-923.

[7] A. Galetin, M. Gertz, J. B. Houston, *Expert Opin. Drug Metab. Toxicol.* **2008**, 4, 909-922.

[8] T. Niwa, N. Murayama, C. Emoto, H. Yamazaki, *Curr. Drug Metab.* **2008**, 9, 20-33.

[9] A. Zimmerlin, M. Trunzer, B. Faller, *Drug Metab. Dispos.* **2011**, 39, 1039-1046.

[10] a) A. Watanabe, K. Nakamura, N. Okudaira, O. Okazaki, K. Sudo. *Drug Metab. Dispos.* **2007**, 35, 1232-1238; b) M. van Dyk, A. J. Kapetas, A. M. Hopkins, A. D. Rodrigues, M. Vourvahis, M. J. Sorich, A. Rowland, *Front Pharmacol.* **2019**, 10, 1120.

[11] a) Li, X. Li, W. Shi, Y. Xu, H. Ma, *Angew. Chem., Int. Ed.* **2018**, 57, 12830-12834; b) H. W. Liu, L. L. Chen, C. Y. Xu, Z. Li, H. Y. Zhang, X. B. Zhang, W. H. Tan, *Chem. Soc. Rev.* **2018**, 47, 7140-7180; c) J. Huang, J. Li, Y. Lyu, Q. Miao, K. Pu, *Nat. Mater.* **2019**, 18, 1133-1143; d) J. J. Zhang, X. Z. Chai, X. P. He, H. J. Kim, J. Y. Yoon, H. Tian, *Chem. Soc. Rev.* **2019**, 48, 683-722; e) H. Zhang, J. L. Fan, J. Y. Wang, S. Z. Zhang, B. R. Dou, X. J. Peng, *J. Am. Chem. Soc.* **2013**, 135, 11663-11669; f) Z. Tian, F. Yan, X. Tian, L. Feng, J. Cui, S. Deng, B. Zhang, T. Xie, S. Huang, X. Ma, *Acta. Pharm. Sin. B.* **2021**, doi: 10.1016/j.apsb.2021.06.004; g) H. D. Li, D. Kim, Q. C. Yao, H. Y. Ge, J. Chung, J. L. Fan, J. Y. Wang, X. J. Peng, J. Y. Yoon, *Angew. Chem. Int. Ed.* **2021**, 60, 17268–17289. h) X. G. Tian, T. Liu, Y. H. Ma, J. Gao, L. Feng, J. N. Cui, T. D. James, X. C. Ma, *Angew. Chem. Int. Ed.* **2021**, 60, 24566-24572.

[12] a) J. Ning, T. Liu, P. Dong, W. Wang, G. Ge, B. Wang, Z. Yu, L. Shi, X. Tian, X. Huo, et al., *J. Am. Chem. Soc.* **2019,** 141, 1126-1134; b) B. Kim, M. Fukuda, J. Y. Lee, D. Su, S. Sanu, A. Silvin, A. T. T. Khoo, T. Kwon, X. Liu, W. Chi, et al., *Angew. Chem., Int. Ed.* **2019**, 58, 7972-7976; c) H. W. Liu, K. Li, X. X. Hu, L. Zhu, Q. Rong, Y. Liu, X. B. Zhang, J. Hasserodt, F. L. Qu, W. Tan, *Angew. Chem., Int. Ed.* **2017**, 56, 11788-11792; d) J. J. Wu, X. Q. Guan, Z. R. Dai, R. J. He, X. X. Ding, L. Yang, G. B. Ge. *Coord. Chem. Rev.* **2021**, 427, 213600; f) L. Feng, J. Ning, X. G. Tian, C. Wang, Z. L. Yu, X. K. Huo, T. Xie, B. J. Zhang, T. D. James, X. C. Ma, *Coord. Chem. Rev.* **2021**, 437, 213740.

[13] N. Chauret, N. Tremblay, R. L. Lackman, J. Y. Gauthier, J. M. Silva, J. Marois, J. A. Yergey, D. A. Nicoll-Griffith, *Anal. Biochem.* **1999**, 276, 215-226.

[14] a) A. B. Renwick, D. F. V. Lewis, S. Fulford, D. Surry, B. Williams, P. D. Worboys, X. Cai, R. W. Wang, R. J. Price, B. G. Lake, et al., *Xenobiotica* **2001**, 31, 187-204; b) D. M. Stresser, S.D. Turner, A. P. Blanchard, V. P. Miller, C. L. Crespi, *Drug Metab. Dispos.* **2002**, 30, 845-852; c) Y. Chen, L. L. Liu, M. Monshouwer, A. J. Fretland, *Drug Metab. Dispos.* **2011**, 39, 2085-2092.

[15] a) J. Ning, W. Wang, G. Ge, P. Chu, F. Long, Y. Yang, Y. Peng, L. Feng, X. Ma, T. D. James. *Angew. Chem., Int. Ed.* **2019**, 58, 9959-9963; b) H. F. Ji, F. L. Ma, Y. P. Dai, X. X. Zhao, K. Xue, S. M. Misal, P. Zhang, Z. J. Qi, H. Y. Zhu, *Sens. Actuators B. Chem.* **2021**, 331, 129372

[16] A. P. Li, U. Doshi, *Drug Metab. Lett.* **2011**, 5, 183-191.

[17] a) S. Ekins, D. M. Stresser, J. A. Williams, *Trends Pharmacol. Sci.* **2003**, 24, 161-166; b) J. E. Bissada, V. Truong, A. A. Abouda, K. J. Wines, R. D. Crouch, K. D. Jackson, *Drug Metab. Dispos.* **2019**, 47, 1257-1269.

[18] N. Garcia-Viloca, J. L. Gao, M. Karplus, D. G. Truhlar, *Science* **2004**, 303, 186-195.

[19] J. Ning, Z. H. Tian, B. Wang, G. B. Ge, Y. An, J. Hou, C. Wang, X. Y. Zhao, Y. N. Li, X. G. Tian, et al., *Mater. Chem. Front.* **2018**, 2, 2013-2020.

[20] a) J. Cui, G. Q. Gao, H. Z. Zhao, Y. Z. Liu, H. L. Nie, X. L. Zhang, *New J. Chem.* **2017**, 41, 11891-11897; b) Y. Y. Chen, L. T. Zhao, H. H. Fu, C. H. Rao, Z. Y. Li, C. X. Liu, *New J. Chem.* **2017**, 41, 8734-8738.

COMMUNICATION
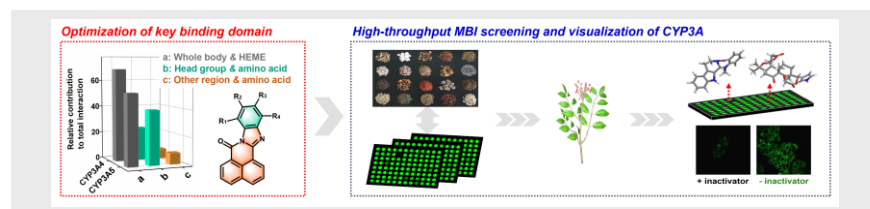
A two-photon fluorescent probe for CYP3A was developed using a rational design strategy that optimized the key binding domain of the fluorophore. The probe semi-quantitatively detects and images CYP3A activity in various living systems, thereby providing a high-throughput screening system facilitating the evaluation of MBI-associated hepatotoxicity by CYP3A.

J. Ning, Z. H. Tian, J. Y. Wang, B. Wang, X. G. Tian, Z. L. Yu, X. K. Huo, L. Feng, J. N. Cui, T. D. James and X. C. Ma**

Page No. – Page No.

Rational Design of a Two-Photon Fluorescent Probe for Human Cytochrome P450 3A and the Visualization of Mechanism-Based Inactivation